

# ViP<sup>2</sup>-CLIP: Visual-Perception Prompting with Unified Alignment for Zero-Shot Anomaly Detection

Ziteng Yang<sup>1\*</sup> Jingzehua Xu<sup>1\*</sup> Yanshu Li<sup>2\*</sup> Zepeng Li<sup>1</sup> Yejiang Wang<sup>1</sup> Xinghui Li<sup>1†</sup>

<sup>1</sup>Tsinghua University <sup>2</sup>Brown University

## Abstract

Zero-shot anomaly detection (ZSAD) aims to detect anomalies without any target domain training samples, relying solely on external auxiliary data. Existing CLIP-based methods attempt to activate the model’s ZSAD potential via handcrafted or static learnable prompts. The former incur high engineering costs and limited semantic coverage, whereas the latter apply identical descriptions across diverse anomaly types, thus fail to adapt to complex variations. Furthermore, since CLIP is originally pretrained on large-scale classification tasks, its anomaly segmentation quality is highly sensitive to the exact wording of class names, severely constraining prompting strategies that depend on class labels. To address these challenges, we introduce ViP<sup>2</sup>-CLIP. The key insight of ViP<sup>2</sup>-CLIP is a Visual-Perception Prompting (ViP-Prompt) mechanism, which fuses global and multi-scale local visual context to adaptively generate fine-grained textual prompts, eliminating manual templates and class-name priors. This design enables our model to focus on precise abnormal regions, making it particularly valuable when category labels are ambiguous or privacy-constrained. Extensive experiments on 15 industrial and medical benchmarks demonstrate that ViP<sup>2</sup>-CLIP achieves state-of-the-art performance and robust cross-domain generalization.

## 1. Introduction

Large-scale vision–language models (VLMs) such as CLIP [23] have shown impressive zero-shot recognition capabilities by pre-training on vast image–text pairs. Inspired by this success, CLIP has been widely adopted for Zero-Shot Anomaly Detection (ZSAD) [12], which seeks to detect anomalies automatically without any target domain training samples, offering a practical solution for data-scarce scenarios. Unlike conventional image classification, which focuses on foreground semantics, anomaly detection empha-

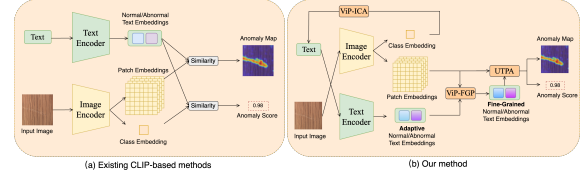


Figure 1. Comparison between prior CLIP-based methods and ViP<sup>2</sup>-CLIP. ViP<sup>2</sup>-CLIP introduces ViP-Prompt to replace fixed class-name tokens with image-conditioned prompts that fuse global and local cues, and employs UTPA to perform a unified patch-level alignment.

sizes irregular regions on object surfaces. Consequently, existing CLIP-based ZSAD methods typically construct two sets of text prompts—‘normal’ and ‘anomalous’, and align them with image features in a shared semantic space. As illustrated in Fig. 1 (a), text prompts are aligned with the global image feature to infer image-level anomaly score, while alignment with local patch features then generates pixel-level anomaly maps.

Currently, state-of-the-art ZSAD methods focus on prompt engineering to leverage CLIP’s generalization. Representative approaches such as WinCLIP [12], Anomaly-CLIP [33], and VCP-CLIP [22] either craft semantically rich manual templates or learn prompt tokens to boost performance. However, manual templates demand extensive human effort and cannot guarantee comprehensive semantic coverage. Although some works [33] introduce object-agnostic learnable prompts to capture generic normal and abnormal concepts, they apply the same description across diverse anomaly types, hindering adaptability to complex semantic variations. Moreover, methods like CLIP-AD [6], AdaCLIP [4], FiLo [8], and KANOCLIP [17] rely heavily on class names as prompt priors. Yet we find that CLIP’s segmentation quality remains acutely sensitive to semantically equivalent class-name variations, even after fine-tuning on auxiliary anomaly data (see Appendix A for detailed analysis). This likely stems from the limited scope of downstream adaptation, which cannot fully stabilize local alignment against label shifts. Such sensitivity constrains

\*Equal contribution.

†Corresponding author.

the class-name usage in prompts, highlighting the urgent need for robust, class-name agnostic but adaptive prompting strategies in ZSAD.

To this end, we propose a Visual-Perception Prompting (ViP-Prompt) mechanism composed of an Image-Conditioned Adapter (ICA) and a Fine-Grained Perception Module (FGP). ICA adaptively injects global visual context into the prompts’ embedding space, while FGP integrates multi-scale patch features, enabling the prompts to capture fine-grained irregularities. By replacing fixed class-name tokens with image-conditioned prompts that fuse global and local cues, ViP-Prompt significantly enhances prompts’ robustness and reinforces cross-modal alignment across diverse semantic scenarios. Building upon that, we further introduce ViP<sup>2</sup>-CLIP, a ZSAD model that integrates visual-perception prompts with a unified alignment mechanism; its overall architecture is depicted in Fig. 1 (b). ViP<sup>2</sup>-CLIP first employs ViP-Prompt to condition text prompts on both global and local visual cues, fully leveraging CLIP’s ZSAD performance; it then adopts a Unified Text-Patch Alignment (UTPA) strategy to align prompt tokens with multi-scale patch features through a single optimization, yielding superior precision in both detection and localization.

Our key contributions are summarized as follows:

- We propose ViP-Prompt, which fuses global and local visual features to generate image-conditioned prompts, fully exploiting CLIP’s potential for ZSAD. This design eliminates the need for handcrafted templates or class-name priors, delivers stronger generalization and robustness, making it particularly valuable when category labels are ambiguous or privacy-constrained.
- On top of that, we present ViP<sup>2</sup>-CLIP, which integrates a simple but effective strategy-UTPA, that for the first time, introduces a consistency-alignment strategy within training-based CLIP models, enhancing CLIP’s performance in both anomaly detection and localization.
- Comprehensive experiments on 15 industrial and medical datasets demonstrate that ViP<sup>2</sup>-CLIP consistently achieves superior ZSAD performance.

## 2. Related Work

**Zero-Shot Anomaly Detection (ZSAD)** ZSAD localizes abnormal regions without any target class samples during training. The advent of CLIP [23] has spurred notable advances in this task. WinCLIP [12] first ported CLIP to ZSAD with diverse handcrafted prompts. However, since CLIP is pretrained to align with general object semantics rather than abnormal patterns, its anomaly detection capability remains limited. To ease this burden, APRIL-GAN [5] and CLIP-AD [6] append shallow linear heads and fine-tune them on auxiliary datasets. AnomalyCLIP [33] removes handcrafted templates via learnable, object-agnostic

prompts, boosting cross-domain generalization, while Ada-CLIP [4] employs hybrid prompts to align text and image features better. VCP-CLIP [22] instead projects the image’s global feature into a fixed handcrafted prompt space, which enhances segmentation performance. By contrast, our ViP-Prompt fuses multi-scale visual cues with a learnable seed to generate dynamic, manual-free prompts, fully exploiting CLIP’s ZSAD performance, boosting both effectiveness and robustness in anomaly detection and localization.

**Prompt Learning** Prompt learning was initially proposed in natural language processing to enhance the adaptability of pre-trained models [21, 28] to diverse downstream tasks. CoOp [23] first brought this paradigm to the vision domain by inserting trainable tokens into text inputs, allowing CLIP to adapt to specific tasks without fine-tuning. Static prompts, however, soon proved brittle on unseen classes. To enhance transferability, CoCoOp [32] and DenseCLIP [24] generate image-conditioned prompts that respond to visual context. Recent works [30, 31] enforce prompt generalization by regularizing learnable tokens toward handcrafted templates, improving unseen class recognition. Works as MaPL [15], PromptSRC [16] and MMRL [9] push prompting into both modalities, jointly tuning image and text space for more substantial cross-modal alignment.

## 3. Preliminary

CLIP consists of a text encoder  $T(\cdot)$  and a visual encoder  $F(\cdot)$ , both implemented as mainstream multi-layer networks. Leveraging contrastive learning on large-scale image-text pairs, CLIP achieves superior zero-shot recognition. Given a class name  $c$ , we combine it with a text prompt template  $G$  (e.g., ‘A photo of a [cls]’, where [cls] represents the category class-name). The resulting text is then fed into the text encoder  $T(\cdot)$  to obtain the prompt embedding  $g_c = T(G(c)) \in \mathbb{R}^D$ . For an input image  $x_i$ , the visual encoder generates its global visual embedding  $f_i \in \mathbb{R}^D$  and the local patch embeddings  $f_i^m \in \mathbb{R}^{H \times W \times D}$ . Specifically, given a category set  $C$ , CLIP computes the probability of image  $x_i$  belonging to  $c$  as follows:

$$p(y = c | x_i) = P(g_c, f_i) = \frac{\exp(\langle g_c, f_i \rangle / \tau)}{\sum_{c' \in C} \exp(\langle g_{c'}, f_i \rangle / \tau)}, \quad (1)$$

where  $\tau$  is a temperature hyperparameter and  $\langle \cdot, \cdot \rangle$  denotes the cosine similarity.

Unlike conventional classification, ZSAD flags deviations from normality rather than assigning foreground semantics. Most approaches, therefore, instantiate two text prompts [12], a normal prompt  $g_n$  and an abnormal prompt  $g_a$ . At the image level, they compare the global image feature  $f_i$  with both prompts and take  $P(g_a, f_i)$  as the anomaly score; while at the pixel level, for each location  $(j, k)$ , they

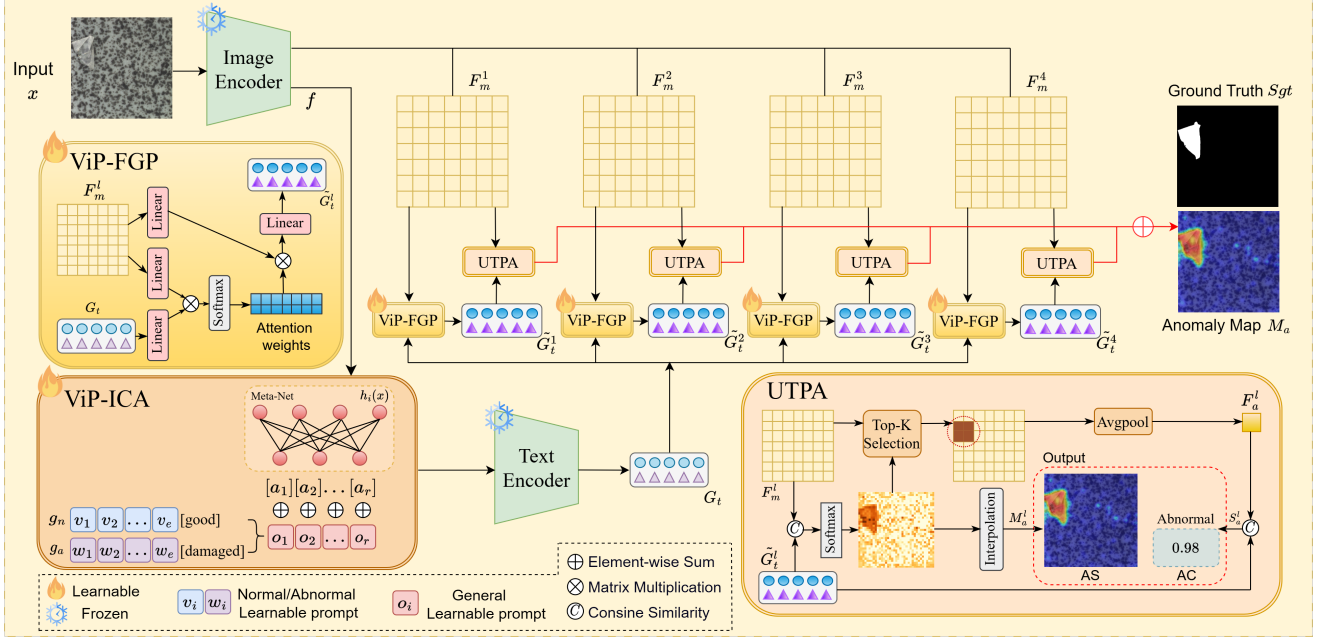


Figure 2. Framework of ViP²-CLIP. ViP²-CLIP first introduces ViP-Prompt to enhance cross-modal alignment: ViP-ICA injects global visual context into the prompts’ embedding space, while ViP-FGP fuses local patch features to enhance the prompts’ fine-grained perceptual capacity. Finally, the UTPA module performs unified alignment in multiple layers to jointly support image-level anomaly detection and pixel-level anomaly localization.

extract the patch token  $f_i^m(j, k)$ , and compute the local normal score  $S_n(j, k) = P(g_n, f_i^m(j, k))$  and anomaly score  $S_a(j, k) = P(g_a, f_i^m(j, k))$ , from which a pixel-wise anomaly map is generated.

## 4. Method

We propose ViP²-CLIP, which leverages Visual-Perception Prompting (ViP-Prompt) to fully exploit CLIP’s ZSAD capabilities. As illustrated in Fig. 2, ViP²-CLIP first introduces ViP-Prompt (Sec. 4.1) to fuse learnable normal and abnormal prompts with both global and multi-scale local visual features. This design enables prompts to adaptively capture the fine-grained visual patterns of the inspected image, thereby improving cross-modal semantic alignment. Furthermore, we adopt a Unified Text-Patch Alignment (UTPA) scoring strategy (Sec. 4.2), which optimizes alignment between prompt tokens and multi-scale patch features to support anomaly detection and localization jointly. By aggregating alignment signals across multiple layers, ViP²-CLIP produces robust anomaly scores and fine-grained anomaly maps.

### 4.1. Visual-Perception Prompt (ViP-Prompt)

We propose ViP-Prompt, an adaptive fine-grained prompting framework, which is built from an Image-Conditioned Adapter (ICA) and Fine-Grained Perception Module (FGP).

By fusing learnable tokens with the global and local visual context, ViP-Prompt generates multi-level descriptions that flexibly track objects’ visual patterns, thus markedly exploiting CLIP’s ZSAD performance in diverse scenarios.

**Image-Conditioned Adapter (ICA)** To eliminate dependence on handcrafted templates and class-name priors, we first define static learnable prompt templates for both normal and anomaly classes:

$$g_n = [v_1][v_2] \dots [v_e] \text{ good } [o_1] \dots [o_r], \quad (2)$$

$$g_a = [w_1][w_2] \dots [w_e] \text{ damaged } [o_1] \dots [o_r], \quad (3)$$

here,  $\{v_i\}, \{w_i\} \in \mathbb{R}^C$  denote the learnable normal and anomaly vector, respectively.  $\{o_i\} \in \mathbb{R}^C$  is a generic learnable token that replaces the explicit class label. We adopt the adjectives ‘good’ and ‘damaged’ to guide the prompts to learn richer normal and anomalous semantics. By autonomously learning  $g_n$  and  $g_a$ , the model can capture generic anomaly patterns across diverse objects.

To condition prompts on the target object and thus adapt to complex detection scenarios, we map the global visual embedding  $f$  extracted by the image encoder through a lightweight Meta-Net  $h_i(\cdot)$  (Linear–ReLU–Linear) into the text embedding space, denoted as  $\{a_i\}_{i=1}^r = h_i(f)$ , where  $r$  is the number of mapped tokens and  $a_i \in \mathbb{R}^C$ , then fuse it with static learnable vector to generate dynamic prompt

token. Thus, we define the prompts' structure as follows:

$$g_n = [v_1][v_2] \dots [v_e] \text{ good } [z_1] \dots [z_r], \quad (4)$$

$$g_a = [w_1][w_2] \dots [w_e] \text{ damaged } [z_1] \dots [z_r], \quad (5)$$

where  $z_i = o_i + a_i$ . By projecting the image's global feature into text embedding space, ICA adaptively generates normal and anomalous descriptors conditioned on the target object, eliminating the dependence on explicit class labels and enabling more robust cross-modal alignment in privacy-constrained settings.

**Fine-Grained Perception Module (FGP)** To further enhance the prompts' fine-grained perceptual capacity, we introduce an attention-based interaction module between the text prompts and multi-scale local image features. Specifically, we project both text embeddings and local patch embeddings into a shared  $C$ -dimensional space. Let  $G_t \in \mathbb{R}^{2 \times C}$  be the prompt embeddings from the text encoder, and  $F_m^l \in \mathbb{R}^{HW \times D}$  be the smoothed local visual embeddings from the  $l$ -th layer of the visual encoder, we then apply three learnable linear mappings to produce query  $Q_t = G_t W_q$ , key  $K_m^l = F_m^l W_k$ , and value  $V_m^l = F_m^l W_v$ , where  $W_q \in \mathbb{R}^{C \times C}$ ,  $W_k, W_v \in \mathbb{R}^{D \times C}$ , are learnable projection matrices.

Then, we compute scaled dot-product attention via  $\text{Softmax}(Q_t K_m^{l\top} / \sqrt{C})$ , and apply these weights to the values  $V_m^l$ , yielding enhanced token embeddings. Finally, a linear projection  $W_o \in \mathbb{R}^{C \times D}$  transforms these embeddings into the layer-specific prompts  $\tilde{G}_t^l$ , which integrate fine-grained local features:

$$\tilde{G}_t^l = (\text{Softmax}(Q_t K_m^{l\top} / \sqrt{C}) V_m^l) W_o, \quad (6)$$

here,  $\tilde{G}_t^l \in \mathbb{R}^{2 \times D}$  comprises the fine-grained normal prompt  $\tilde{g}_n$  and anomalous prompt  $\tilde{g}_a$ .

To assess FGP's fine-grained sensitivity, Fig. 3 visualizes the attention maps of both normal and abnormal prompts across diverse images. Normal prompts activate on regular textures and structures of the image, while anomalous prompts concentrate on defects and irregular regions, indicating high sensitivity to anomalous patterns. These results demonstrate that FGP effectively refines prompt embeddings by incorporating localized visual cues, thereby enhancing cross-modal alignment.

## 4.2. Unified Text-Patch Alignment (UTPA)

Recent CLIP-based ZSAD models typically adopt a dual-branch alignment scheme [5, 6, 33]: one branch aligns the text prompt with global visual embedding to score anomalies at the image level, while the other aligns it with local patch embeddings for pixel-level anomaly maps. However, because these branches operate in separate feature

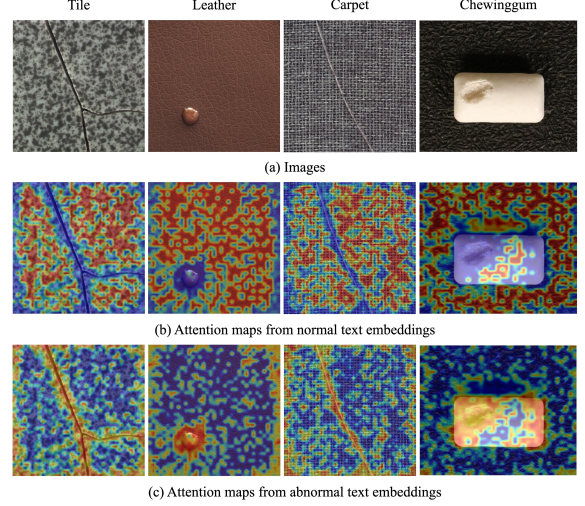


Figure 3. The visualization result of the attention maps from different prompts in our FGP module.

subspaces, it hinders the simultaneous attainment of high-precision anomaly detection and localization.

To address this limitation, we introduce the UTPA strategy, which treats anomaly detection and localization as a unified alignment task between text embeddings and local patch embeddings. Concretely, to obtain the pixel-level anomaly map, we follow the standard practice: for the  $l$ -th layer feature map  $F_m^l$ , the patch token at spatial location  $(j, k)$ , denoted as  $f_{j,k}^l \in \mathbb{R}^D$ , receives its anomaly score by computing the similarity  $P(\tilde{g}_a, f_{j,k}^l)$ , as defined in Eq. (1).

Next, we upsample the anomaly scores of all patch tokens to produce the anomaly map  $M_a^l$ :

$$M_a^l = \text{Up}(P(\tilde{g}_a, F_m^l)), \quad (7)$$

where  $\text{Up}(\cdot)$  denotes channel-wise upsampling.

Unlike prior works [5, 6, 33] that rely on global alignment, we contend that an image's abnormality is driven by its most defective regions. Consequently, our image-level score is still derived from local patch features. For the  $l$ -th layer feature map  $F_m^l$ , we select the Top-k patch tokens with the highest  $P(\tilde{g}_a, f_{j,k}^l)$  among all patches. The image's representative anomaly feature  $F_a^l$  is then obtained via global average pooling over this subset:

$$F_a^l = \frac{1}{k} \sum_{(j,k) \in \mathcal{T}_l} f_{j,k}^l, \quad (8)$$

where  $\mathcal{T}_l$  indexes the chosen Top-k patches. The Top-k pooling directs the model's attention to the most suspicious patches, ensuring that the subsequent anomaly score faithfully reflects the severity of localized defects. Consequently, the image-level anomaly score  $S_a^l$  at the  $l$ -th layer



is obtained by computing  $S_a^l = P(\tilde{g}_a, F_a^l)$ . By enforcing a unified text-patch alignment, UTPA effectively overcomes the optimization conflict of traditional dual-branch schemes, yielding more balanced ZSAD performance, as further validated in Sec. 5.3.

### 4.3. Training and Inference

During training, ViP<sup>2</sup>-CLIP is optimized by minimizing a global loss  $L_{\text{global}}$  and a local loss  $L_{\text{local}}$  [33]:

$$L_{\text{total}} = L_{\text{global}} + \lambda \sum_{l=1}^N L_{\text{local}}^l, \quad (9)$$

here,  $\lambda$  is a hyperparameter to balance the global and local losses;  $N$  represents the number of intermediate layers.  $L_{\text{global}}$  is the cross-entropy loss matching the cosine similarity between text embeddings  $\tilde{g}_n/\tilde{g}_a$  and the representative anomalous visual feature  $F_a^l$ ;  $L_{\text{local}}$  is computed as the sum of a Focal loss [19] and a Dice loss [18] to optimize local alignment jointly:

$$\begin{aligned} L_{\text{local}} = & \text{Focal}(\text{Up}([M_n^l, M_a^l]), S_{\text{gt}}) \\ & + \text{Dice}(\text{Up}(M_n^l), I - S_{\text{gt}}) \\ & + \text{Dice}(\text{Up}(M_a^l), S_{\text{gt}}), \end{aligned} \quad (10)$$

where  $[\cdot, \cdot]$  denotes channel-wise concatenation; for each layer  $l$ ,  $M_n^l$  and  $M_a^l$  are the normal and anomaly score maps;  $S_{\text{gt}}$  is the ground-truth mask; and  $I$  is the all-ones matrix.

During inference, the final image-level anomaly score is computed as:  $\text{Score} = \frac{1}{N} \sum_{l=1}^N S_a^l$ . For pixel-level prediction, we merge all intermediate maps  $M_n^l$  and  $M_a^l$ , then obtain the anomaly map  $\text{Map} \in \mathbb{R}^{H \times W}$  as follows:

$$\text{Map} = G_\sigma \left( \frac{1}{N} \sum_{l=1}^N \left( \frac{1}{2} (I - \text{Up}(M_n^l)) + \frac{1}{2} \text{Up}(M_a^l) \right) \right) \quad (11)$$

where  $G_\sigma$  denotes Gaussian smoothing.

## 5. Experiments

### 5.1. Setup

**Datasets & Baselines** To comprehensively evaluate ViP<sup>2</sup>-CLIP across diverse application scenarios, we conduct extensive experiments on public benchmarks spanning industrial and medical domains. In the industrial domain, we use MVTec AD [2], VisA [34], MPDD [13], BTAD [20], KSDD [26], DAGM [29], and DTD-Synthetic [1]. For medical imaging, we include brain tumour detection datasets HeadCT [25], BrainMRI [25], and Br35H [10], skin cancer detection dataset ISIC [7], colon polyp detection datasets CVC-ClinicDB [3], CVC-ColonDB [27], Endo [11], and Kvasir [14]. We compare ViP<sup>2</sup>-CLIP against five leading

ZSAD methods: CLIP [23], WinCLIP [12], APRIL-GAN [5], AnomalyCLIP [33] and AdaCLIP [4]. More details about the datasets or methods are shown in Appendix B.

**Metrics** We adopt standard metrics for evaluation: for image-level anomaly detection, we report the Area Under the Receiver Operating Characteristic curve (AUROC), Average Precision (AP), and maximum F1 (F1); for pixel-level anomaly segmentation, we report AUROC, the Area Under the Per-Region Overlap curve (AUPRO), and F1.

**Implementation Details** We use the publicly released CLIP (ViT-L/14@336px) as the frozen backbone. The learnable prompts contain 10 tokens, 3 of which interact explicitly with the global visual embedding. In UTPA, we retain the top 50 anomalous patches at each alignment layer as image-level descriptors and, following prior work [4, 33], apply cross-modal alignment at layers 6, 12, 18, and 24. We fine-tune ViP<sup>2</sup>-CLIP on MVTec AD's test split and evaluate ZSAD performance on all other datasets; for MVTec AD, we fine-tune on VisA's test set. Dataset-level metrics are averaged across all subclasses. All experiments are implemented in PyTorch 2.6.0 on a single NVIDIA L20 (48 GB). Further implementation details are provided in Appendix B.

### 5.2. Main Results

#### Zero-Shot Anomaly Detection on Industrial Datasets

Tab. 1 compares ViP<sup>2</sup>-CLIP against five representative baselines on seven industrial defect benchmarks. Our model delivers competitive results and outperforms all baselines in most datasets. The vanilla CLIP struggles, as its pre-training emphasizes general object semantics rather than anomaly patterns. WinCLIP and APRIL-GAN improve detection through handcrafted prompts and local features tuning. AnomalyCLIP employs object-agnostic prompts but remains limited by static prompt design and shallow cross-modal fusion. AdaCLIP further refines prompts in both visual and textual space, which boosts F1 but neglects AUPRO, leading to an imbalanced ZSAD. In contrast, ViP<sup>2</sup>-CLIP yields consistent improvements across all metrics, achieving state-of-the-art performance. Our ViP-Prompt creates fine-grained normal and abnormal prompts that align tightly with object features; paired with UTPA's unified alignment, it markedly boosts accuracy at both image-level detection and pixel-level localization. Fig. 4 compares the anomaly detection results of our approach with four strong baselines, showing that ViP<sup>2</sup>-CLIP more accurately captures defects with sharper boundaries, supporting the observed quantitative gains. We also provide failure cases analyses in Appendix C.

#### Zero-Shot Anomaly Detection on Medical Datasets

To assess cross-domain transferability, we benchmark ViP<sup>2</sup>-

Task	Datasets	C	CLIP	WinCLIP	APRIL-GAN	AnomalyCLIP	AdaCLIP	ViP <sup>2</sup> -CLIP
			OpenCLIP	CVPR 2023	CVPRw 2023	ICLR 2024	ECCV 2024	-
Image-level (AUROC, AP, F1)	MVTec AD	15	(66.5, 82.6, 86.7)	(91.8, 96.5, 92.7)*	(86.1, 93.5, 90.4)	(91.6, 96.4, 92.7)	(90.1, 95.6, 92.3)	(91.2, 96.0, 92.0)
	VisA	12	(60.2, 66.2, 73.0)	(78.1, 81.2, 78.2)*	(77.5, 80.9, 78.7)	(82.0, 85.3, 80.4)	(87.2, 89.7, 83.5)	(88.5, 90.4, 84.8)
	MPDD	6	(58.7, 69.7, 76.0)	(61.5, 69.2, 77.5)	(76.8, 83.0, 81.0)	(77.5, 82.5, 80.4)	(74.8, 78.6, 83.3)	(79.7, 84.5, 82.4)
	KSDD	1	(74.3, 55.3, 57.8)	(92.4, 82.9, 77.7)	(96.5, 91.2, 85.4)	(97.8, 94.2, 89.7)	(97.2, 92.6, 89.5)	(98.1, 95.8, 93.2)
	BTAD	3	(25.7, 49.8, 66.0)	(68.2, 70.9, 67.8)	(73.7, 69.7, 68.2)	(88.2, 88.2, 83.8)	(89.3, 96.5, 90.9)	(95.0, 98.4, 94.7)
	DAGM	10	(55.3, 43.2, 49.6)	(91.8, 79.5, 75.7)	(94.4, 83.9, 80.2)	(97.7, 92.4, 90.1)	(98.2, 92.3, 90.9)	(98.5, 94.3, 92.6)
	DTD-Synthetic	12	(52.3, 77.8, 85.1)	(95.1, 97.7, 94.1)	(85.6, 94.0, 89.1)	(93.9, 97.2, 93.6)	(96.3, 98.1, 95.5)	(95.5, 98.1, 94.3)
	AVERAGE	-	(56.1, 63.5, 70.6)	(82.1, 82.1, 80.5)	(84.4, 85.2, 81.9)	(89.8, 90.9, 87.2)	(90.4, 91.9, 89.4)	(92.4, 93.9, 90.6)
Pixel-level (AUROC, PRO, F1)	MVTec AD	15	(35.6, 10.6, 6.9)	(85.1, 64.6, 24.8)*	(87.6, 44.0, 43.3)	(91.1, 81.4, 39.1)	(89.6, 37.8, 45.1)	(90.5, 87.1, 43.1)
	VisA	12	(43.6, 14.0, 1.5)	(79.6, 56.8, 9.0)*	(94.2, 86.6, 32.3)	(95.5, 86.7, 28.3)	(95.5, 56.8, 37.0)	(95.4, 92.2, 33.6)
	MPDD	6	(56.2, 27.3, 8.2)	(71.2, 40.5, 15.4)	(94.3, 83.8, 31.3)	(96.5, 88.7, 34.2)	(96.1, 60.3, 31.9)	(97.2, 92.6, 35.9)
	KSDD	1	(21.7, 2.6, 0.5)	(92.8, 70.3, 15.8)	(93.2, 84.1, 43.6)	(98.1, 94.9, 56.5)	(98.4, 53.0, 52.8)	(98.5, 96.2, 53.0)
	BTAD	3	(41.2, 10.8, 6.8)	(72.7, 27.5, 18.5)	(89.3, 68.7, 40.6)	(94.2, 75.4, 49.7)	(90.7, 22.3, 51.4)	(95.6, 86.1, 52.7)
	DAGM	10	(49.6, 12.4, 2.4)	(87.6, 65.7, 12.7)	(82.4, 66.0, 37.4)	(95.6, 91.0, 58.9)	(94.3, 42.5, 59.6)	(97.5, 95.2, 61.2)
	DTD-Synthetic	12	(43.8, 16.0, 3.7)	(79.5, 51.4, 16.1)	(95.2, 87.3, 67.4)	(97.9, 92.0, 62.2)	(98.5, 75.0, 71.8)	(99.0, 96.5, 67.5)
	AVERAGE	-	(41.7, 13.4, 4.3)	(79.9, 52.6, 16.0)	(90.9, 74.4, 42.2)	(95.6, 87.2, 47.0)	(94.7, 49.7, 49.9)	(96.2, 92.3, 49.6)

Table 1. ZSAD performance comparison on industrial domain. \* denotes results taken from original papers. The best performance is shown in red, with the second-best highlighted in blue.

Task	Datasets	C	CLIP	WinCLIP	APRIL-GAN	AnomalyCLIP	AdaCLIP	ViP <sup>2</sup> -CLIP
			OpenCLIP	CVPR 2023	CVPRw 2023	ICLR 2024	ECCV 2024	-
Image-level (AUROC, AP, F1)	HeadCT	1	(67.8, 62.4, 70.9)	(81.8, 80.2, 78.9)	(89.1, 89.4, 82.1)	(93.0, 91.1, 88.4)	(94.0, 91.4, 90.1)	(94.3, 93.9, 88.1)
	BrainMRI	1	(72.2, 81.5, 76.5)	(86.6, 91.5, 84.1)	(89.4, 91.0, 88.2)	(90.0, 92.1, 86.5)	(94.3, 95.5, 92.2)	(95.3, 96.7, 92.3)
	Brain35H	1	(76.3, 77.7, 72.2)	(79.9, 82.2, 74.0)	(91.6, 92.1, 84.5)	(93.4, 93.8, 86.4)	(95.7, 95.8, 91.1)	(95.8, 96.0, 90.1)
	AVERAGE	-	(72.1, 73.9, 73.2)	(82.8, 84.6, 79.0)	(90.0, 90.8, 84.9)	(92.1, 92.3, 87.1)	(94.7, 94.2, 91.1)	(95.1, 95.5, 90.2)
Pixel-level (AUROC, PRO, F1)	ISIC	1	(43.2, 7.6, 44.0)	(83.3, 55.1, 64.1)	(89.4, 77.2, 71.4)	(89.4, 78.4, 71.6)	(91.3, 53.2, 75.5)	(90.3, 82.3, 73.7)
	CVC-ColonDB	1	(59.8, 30.4, 17.8)	(64.8, 28.4, 21.0)	(78.4, 64.6, 29.7)	(81.9, 71.2, 37.5)	(81.5, 64.3, 33.6)	(82.5, 74.8, 36.2)
	CVC-ClinicDB	1	(63.1, 33.8, 23.4)	(70.3, 32.5, 27.2)	(80.5, 60.7, 38.7)	(82.9, 68.1, 42.4)	(83.9, 65.7, 42.3)	(86.3, 72.1, 44.9)
	Endo	1	(59.7, 25.2, 28.9)	(68.2, 28.3, 32.9)	(81.9, 54.9, 44.8)	(84.2, 63.4, 50.3)	(86.0, 63.4, 51.8)	(84.5, 63.7, 49.2)
	Kvasir	1	(58.0, 18.3, 29.3)	(69.7, 24.5, 35.9)	(75.0, 36.3, 40.0)	(79.0, 45.4, 46.2)	(81.6, 49.1, 47.1)	(81.9, 47.8, 47.3)
	AVERAGE	-	(56.8, 23.1, 28.7)	(71.3, 33.8, 36.2)	(81.0, 58.7, 44.9)	(83.5, 65.3, 49.6)	(84.9, 59.1, 50.1)	(85.1, 68.1, 50.3)

Table 2. ZSAD performance comparison on medical domain. The best performance is shown in red, with the second-best highlighted in blue. Note that the image-level medical AD datasets do not provide pixel-level segmentation annotations, so the pixel-level medical AD datasets are different from the image-level datasets.

CLIP on eight public medical defect datasets. As shown in Tab. 2, ViP<sup>2</sup>-CLIP achieves consistently superior detection performance on most medical datasets, generally outperforming prior methods. Qualitative examples in Fig. 4 further support this claim: our model precisely localizes melanoma lesions in dermoscopy images and colonic polyps in endoscopic frames, demonstrating robust adaptability to disparate pathological patterns.

**Static prompts vs. Visual-Perception prompts** To quantify the benefit of visual conditioning, we compare ViP<sup>2</sup>-CLIP against ViP<sup>2</sup>-CLIP<sub>re</sub>, which only uses static learnable prompts without visual cues. Fig. 5 reports image-level and pixel-level F1 gains on the seven industrial datasets. ViP<sup>2</sup>-CLIP achieves higher pixel-level F1 on all datasets and improves image-level F1 on five of them. The slight drops on BTAD and DAGM are attributed to significant domain shifts from MVTec AD: BTAD features real-world industrial environments with complex lighting conditions, while DAGM contains synthetic textures with small, repetitive anomalies. These differences likely cause shifts in global visual embeddings, limiting ICA’s transferability and

Model	Training Time (h)	Inference Time (ms)	GPU Cost (GB)	Trainable Parameters (M)
AnomalyCLIP	1.02	90.72 ± 0.16	2.75	5.56
AdaCLIP	2.24	134.20 ± 0.39	3.17	10.67
ViP <sup>2</sup> -CLIP	0.54	48.69 ± 0.19	2.21	4.15

Table 3. Comparison of computational efficiency on VisA.

UTPA	ViP-Prompt ICA	FGP	MVTec AD		VisA	
			Pixel-level	Image-level	Pixel-level	Image-level
			(37.8, 11.5, 7.0)	(74.1, 87.6, 87.2)	(43.5, 14.6, 2.8)	(60.2, 66.3, 74.5)
	✓		(89.5, 79.9, 38.6)	(71.8, 86.2, 88.5)	(95.2, 90.9, 31.6)	(79.7, 82.8, 79.5)
		✓	(90.0, 85.5, 42.7)	(66.1, 82.6, 86.6)	(95.3, 91.5, 33.4)	(60.1, 66.4, 73.2)
	✓	✓	(87.7, 83.8, 42.4)	(88.9, 94.9, 91.6)	(95.2, 91.6, 35.5)	(83.0, 85.9, 81.4)
	✓	✓	(89.8, 84.4, 40.2)	(89.2, 95.0, 91.4)	(94.9, 91.4, 31.3)	(86.3, 89.1, 83.8)
	✓	✓	(88.8, 82.1, 38.7)	(85.2, 93.3, 89.0)	(95.3, 91.9, 31.4)	(87.6, 89.4, 83.8)
	✓	✓	(90.5, 87.1, 43.1)	(91.2, 96.0, 92.0)	(95.4, 92.2, 33.6)	(88.5, 90.4, 84.8)

Table 4. Module ablation.

leading to imbalanced detection performance. This underscores the importance of domain consistency in transfer learning, as large domain gaps can hinder generalization. Despite minor image-level drops on a few datasets, ViP-Prompt consistently achieves SOTA performance across diverse detection scenarios, demonstrating that incorporating both global and local visual cues into prompts enhances cross-modal alignment and promotes robust generalization.

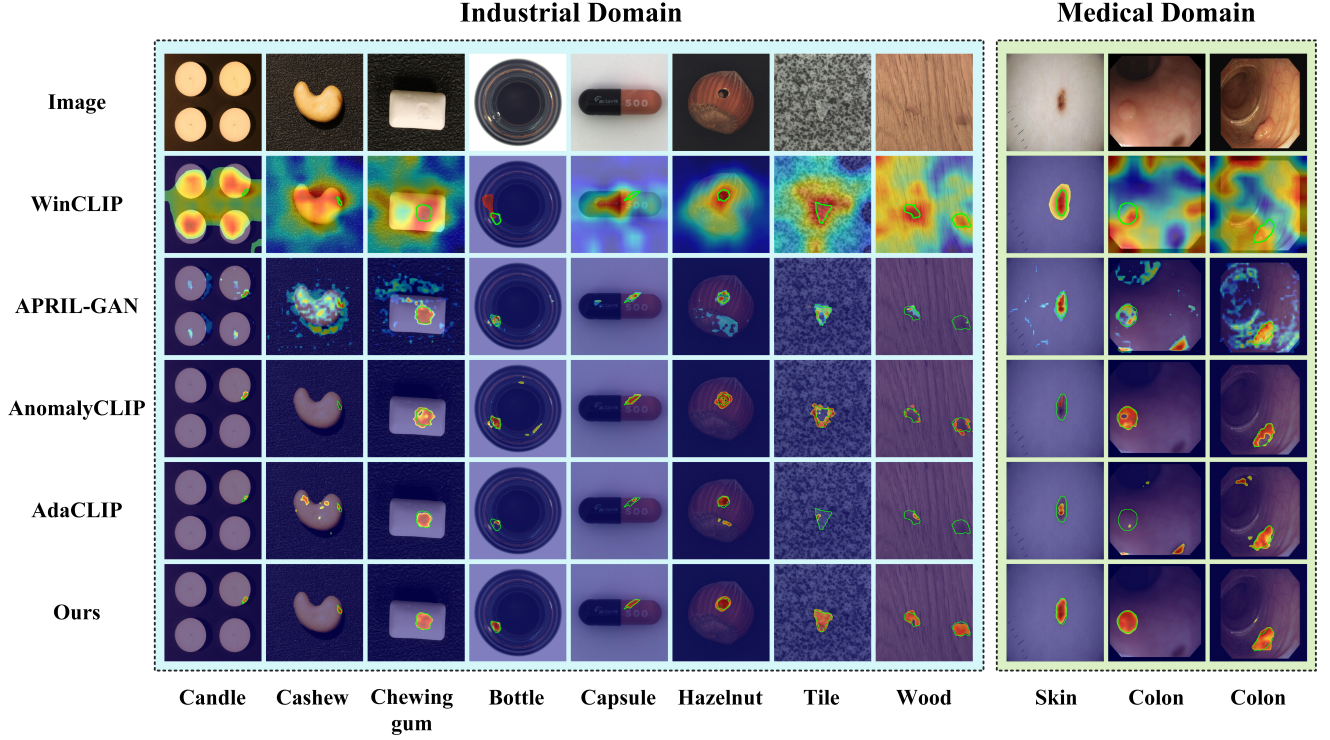


Figure 4. Visualization of anomaly maps of different ZSAD methods. Our proposed ViP<sup>2</sup>-CLIP achieves the sharpest segmentations, capturing fine-grained defects in both industrial and medical datasets.

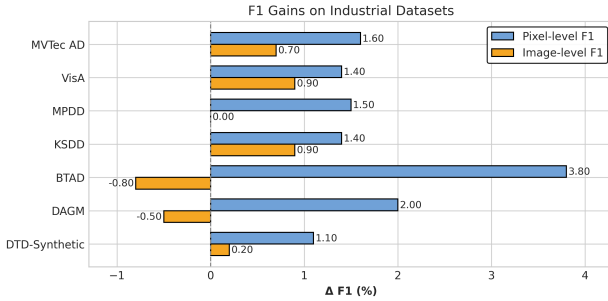


Figure 5. F1 gains of using visual-conditioned prompts compared to static learnable prompts.

**Computational Efficiency Analysis** Tab. 3 compares the computational efficiency of the top three baselines. AnomalyCLIP modifies self-attention weights via DPAM, while AdaCLIP introduces additional learnable tokens and a multi-scale clustering module, both of which increase computational overhead. In contrast, ViP<sup>2</sup>-CLIP employs only two lightweight adapters outside the frozen CLIP backbone, achieving the fastest training (0.54 h), inference (48.7 ms/image), and the lowest GPU memory usage (2.21 GB), making it well-suited for deployment in resource-

Module	MVTec AD		VisA	
	Pixel-level	Image-level	Pixel-level	Image-level
CLIP_DUAL	(69.6, 24.6, 12.0)	(88.6, 94.9, 91.3)	(93.3, 82.4, 24.2)	(79.3, 82.4, 79.0)
CLIP_UTPA	(89.6, 83.7, 37.4)	(85.0, 93.3, 88.8)	(94.4, 88.4, 26.2)	(83.8, 86.7, 81.4)

Table 5. Ablation on the effectiveness of UTPA.

constrained industrial environments.

### 5.3. Ablation Study & Discussion

**Module Ablation** We isolate the contributions of three key components: ViP-ICA, ViP-FGP, and UTPA. Tab. 4 shows that adding each module yields a clear, consistent gain, validating their standalone effectiveness. Specifically, ICA adaptively injects global visual context into prompt embeddings, while FGP incorporates fine-grained local cues, enabling the prompts to capture precise irregularities. Furthermore, UTPA consistently improves both detection and localization performance upon integration, demonstrating the general effectiveness of the unified patch-level alignment strategy in guiding prompt learning toward more discriminative representations.

**UTPA for Resolving Optimization Conflicts** We conduct an ablation study using a frozen CLIP backbone with

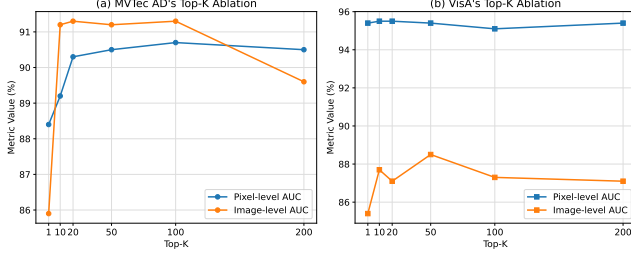


Figure 6. Top-k component ablation.

learnable prompts for normal and anomalous classes to evaluate the effectiveness of UTPA in guiding network learning. The baseline (CLIP\_DUAL) adopts a dual-branch strategy that aligns prompts with both global and local visual embeddings. In contrast, CLIP\_UTPA simplifies the optimization by aligning solely with local features. As shown in Tab. 5, on the MVTec AD dataset, the dual-branch strategy tends to overfit image-level scores while underperforming on pixel-level detection. UTPA, by comparison, achieves more stable and superior results. As for VisA, it outperforms the baseline across both pixel- and image-level metrics. Several results in Tab. 4 also support this observation: traditional dual-branch approaches often suffer from imbalanced performance due to conflicting objectives, whereas UTPA alleviates this issue through consistent text-patch alignment. This facilitates more robust model learning and provides a novel alignment paradigm for more accurate ZSAD research.

**Top-K Ablation** To assess how the image-level representation is affected by the number of anomalous patches, we vary  $K \in \{1, 10, 20, 50, 100, 200\}$  and examine the AUROC performance in Fig. 6. At  $K = 1$ , the model is overly sensitive to local noise, yielding a low AUROC. As  $K$  increases, performance steadily improves, demonstrating that aggregating multiple high-scoring anomalous patches enhances robustness. On MVTec AD, performance plateaus when  $K$  is at 50 or 100; As for VisA, the optimum occurs at  $K = 50$ . Beyond these points, additional patches introduce mostly normal regions, diluting the anomaly signals and reducing accuracy. Balanced across all metrics, we select the top 50 most anomalous patches as image-level descriptors, which aligns well with the anomaly distribution characteristics in most detection scenarios.

**Feature Visualization at Different layers** To investigate the role of network depth in capturing anomalous features, Fig. 7 presents anomaly maps derived from  $F_m^1$  to  $F_m^4$  layers. We observe that for complex object categories such as hazelnut, deeper layers yield more accurate anomaly localization. In contrast, for simpler texture-based objects like leather, intermediate layers offer sufficient dis-

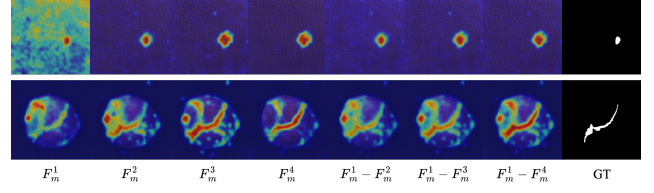


Figure 7. Visualization of anomaly maps from different layers.

State words	MVTec AD		VisA	
	Pixel-level	Image-level	Pixel-level	Image-level
Good/Damage	(90.5, 87.1, 43.1)	(91.2, 96.0, 92.0)	(95.4, 92.2, 33.6)	(88.5, 90.4, 84.8)
Normal/Abnormal	(90.6, 87.5, 43.6)	(91.1, 95.9, 92.3)	(95.3, 91.9, 33.3)	(88.3, 90.2, 84.5)
Perfect/Flawed	(90.4, 87.2, 43.7)	(91.7, 96.2, 92.5)	(95.4, 92.0, 33.5)	(88.3, 90.3, 84.5)
Flawless/Imperfect	(90.4, 87.4, 43.3)	(91.2, 95.9, 92.2)	(95.4, 91.9, 33.1)	(87.9, 90.2, 84.3)

Table 6. Ablation on different state words in prompts.

criminative power. Aggregating features across multiple depths provides complementary contextual cues, allowing the model to better adapt to diverse anomaly types, and thereby achieve more robust anomaly detection.

**State-Adjective Ablation** To verify our prompt’s robustness, we replace the original ‘good/damaged’ adjectives with several alternative pairs of similar meaning and retrain the model on MVTec-AD and VisA. As Tab. 6 shows, detection performance remains consistent across all variants, demonstrating insensitivity to specific adjective choices. This resilience stems from our learnable prompt tokens, which autonomously capture normal and anomalous semantics, obviating the need for handcrafted text templates.

## 6. Conclusion

We propose ViP<sup>2</sup>-CLIP, a universal ZSAD framework that detects anomalies in unseen categories without any target domain training samples. At its core, ViP-Prompt adaptively integrates global and local visual cues into text prompts, eliminating reliance on manual templates or class-name priors, achieving superior generalization and robustness in cross-modal alignment. In addition, the UTPA strategy optimizes a unified text–patch alignment across scales, sharpening both detection and localization performance. Extensive experiments on 15 mainstream datasets demonstrate that ViP<sup>2</sup>-CLIP consistently outperforms existing methods across various detection scenarios, especially when category labels are ambiguous or privacy-constrained, offering a more accurate and scalable solution for ZSAD.

## References

- [1] Toshimichi Aota, Lloyd Teh Tzer Tong, and Takayuki Okatani. Zero-shot versus many-shot: Unsupervised texture anomaly detection. In *Proceedings of the IEEE/CVF Winter Conference on Applications of Computer Vision*, pages 5564–5572, 2023. 5



- [2] Paul Bergmann, Michael Fauser, David Sattlegger, and Carsten Steger. Mvtec ad—a comprehensive real-world dataset for unsupervised anomaly detection. In *Proceedings of the IEEE/CVF conference on computer vision and pattern recognition*, pages 9592–9600, 2019. 5
- [3] Jorge Bernal, F Javier Sánchez, Gloria Fernández-Esparrach, Debora Gil, Cristina Rodríguez, and Fernando Vilariño. Wm-dova maps for accurate polyp highlighting in colonoscopy: Validation vs. saliency maps from physicians. *Computerized medical imaging and graphics*, 43:99–111, 2015. 5
- [4] Yunkang Cao, Jiangning Zhang, Luca Frittoli, Yuqi Cheng, Weiming Shen, and Giacomo Boracchi. Adacclip: Adapting clip with hybrid learnable prompts for zero-shot anomaly detection. In *European Conference on Computer Vision*, pages 55–72. Springer, 2024. 1, 2, 5
- [5] Xuhai Chen, Yue Han, and Jiangning Zhang. A zero-few-shot anomaly classification and segmentation method for cvpr 2023 vand workshop challenge tracks 1&2. *1st Place on Zero-shot AD and 4th Place on Few-shot AD*, 2305:17382, 2023. 2, 4, 5
- [6] Xuhai Chen, Jiangning Zhang, Guanzhong Tian, Haoyang He, Wuhao Zhang, Yabiao Wang, Chengjie Wang, and Yong Liu. Clip-ad: A language-guided staged dual-path model for zero-shot anomaly detection. In *International Joint Conference on Artificial Intelligence*, pages 17–33. Springer, 2024. 1, 2, 4
- [7] Noel CF Codella, David Gutman, M Emre Celebi, Brian Helba, Michael A Marchetti, Stephen W Dusza, Aadi Kalloo, Konstantinos Liopyris, Nabin Mishra, Harald Kittler, et al. Skin lesion analysis toward melanoma detection: A challenge at the 2017 international symposium on biomedical imaging (isbi), hosted by the international skin imaging collaboration (isic). In *2018 IEEE 15th international symposium on biomedical imaging (ISBI 2018)*, pages 168–172. IEEE, 2018. 5
- [8] Zhaopeng Gu, Bingke Zhu, Guibo Zhu, Yingying Chen, Hao Li, Ming Tang, and Jinqiao Wang. Filo: Zero-shot anomaly detection by fine-grained description and high-quality localization. In *Proceedings of the 32nd ACM International Conference on Multimedia*, pages 2041–2049, 2024. 1
- [9] Yuncheng Guo and Xiaodong Gu. Mmrl: Multi-modal representation learning for vision-language models. In *Proceedings of the Computer Vision and Pattern Recognition Conference*, pages 25015–25025, 2025. 2
- [10] Ahmed Hamada. BR35H: Brain Tumor Detection 2020. <https://www.kaggle.com/datasets/ahmedhamada0/brain-tumor-detection>, 2020. Accessed: 2025-05-07. 5
- [11] Steven A Hicks, Debesh Jha, Vajira Thambawita, Pål Halvorsen, Hugo L Hammer, and Michael A Riegler. The endotect 2020 challenge: evaluation and comparison of classification, segmentation and inference time for endoscopy. In *Pattern Recognition. ICPR International Workshops and Challenges: Virtual Event, January 10-15, 2021, Proceedings, Part VIII*, pages 263–274. Springer, 2021. 5
- [12] Jongheon Jeong, Yang Zou, Taewan Kim, Dongqing Zhang, Avinash Ravichandran, and Onkar Dabeer. Winclip: Zero-few-shot anomaly classification and segmentation. In *Proceedings of the IEEE/CVF Conference on Computer Vision and Pattern Recognition*, pages 19606–19616, 2023. 1, 2, 5
- [13] Stepan Jezek, Martin Jonak, Radim Burget, Pavel Dvorak, and Milos Skotak. Deep learning-based defect detection of metal parts: evaluating current methods in complex conditions. In *2021 13th International congress on ultra modern telecommunications and control systems and workshops (ICUMT)*, pages 66–71. IEEE, 2021. 5
- [14] D Jha, PH Smedsrud, MA Riegler, P Halvorsen, T De Lange, D Johansen, and HD Johansen. Kvasir-seg: A segmented polyp dataset. multimedia modeling. *MMM 2020. Lecture Notes in Computer Science*, 11962, 2019. 5
- [15] Muhammad Uzair Khattak, Hanoona Rasheed, Muhammad Maaz, Salman Khan, and Fahad Shahbaz Khan. Maple: Multi-modal prompt learning. In *Proceedings of the IEEE/CVF conference on computer vision and pattern recognition*, pages 19113–19122, 2023. 2
- [16] Muhammad Uzair Khattak, Syed Talal Wasim, Muzammal Naseer, Salman Khan, Ming-Hsuan Yang, and Fahad Shahbaz Khan. Self-regulating prompts: Foundational model adaptation without forgetting. In *Proceedings of the IEEE/CVF international conference on computer vision*, pages 15190–15200, 2023. 2
- [17] Chengyuan Li, Suyang Zhou, Jieping Kong, Lei Qi, and Hui Xue. Kanoclip: Zero-shot anomaly detection through knowledge-driven prompt learning and enhanced cross-modal integration. *arXiv preprint arXiv:2501.03786*, 2025. 1
- [18] Xiaoya Li, Xiaofei Sun, Yuxian Meng, Junjun Liang, Fei Wu, and Jiwei Li. Dice loss for data-imbalanced nlp tasks. *arXiv preprint arXiv:1911.02855*, 2019. 5
- [19] Tsung-Yi Lin, Priya Goyal, Ross Girshick, Kaiming He, and Piotr Dollár. Focal loss for dense object detection. In *Proceedings of the IEEE international conference on computer vision*, pages 2980–2988, 2017. 5
- [20] Pankaj Mishra, Riccardo Verk, Daniele Fornasier, Claudio Picciarelli, and Gian Luca Foresti. Vt-adl: A vision transformer network for image anomaly detection and localization. In *2021 IEEE 30th International Symposium on Industrial Electronics (ISIE)*, pages 01–06. IEEE, 2021. 5
- [21] Long Ouyang, Jeffrey Wu, Xu Jiang, Diogo Almeida, Carroll Wainwright, Pamela Mishkin, Chong Zhang, Sandhini Agarwal, Katarina Slama, Alex Ray, et al. Training language models to follow instructions with human feedback. *Advances in neural information processing systems*, 35:27730–27744, 2022. 2
- [22] Zhen Qu, Xian Tao, Mukesh Prasad, Fei Shen, Zhengtao Zhang, Xinyi Gong, and Guiguang Ding. Vcp-clip: A visual context prompting model for zero-shot anomaly segmentation. In *European Conference on Computer Vision*, pages 301–317. Springer, 2024. 1, 2
- [23] Alec Radford, Jong Wook Kim, Chris Hallacy, Aditya Ramesh, Gabriel Goh, Sandhini Agarwal, Girish Sastry, Amanda Askell, Pamela Mishkin, Jack Clark, et al. Learning transferable visual models from natural language supervision. In *International conference on machine learning*, pages 8748–8763. Pmlr, 2021. 1, 2, 5

- [24] Yongming Rao, Wenliang Zhao, Guangyi Chen, Yansong Tang, Zheng Zhu, Guan Huang, Jie Zhou, and Jiwen Lu. Denseclip: Language-guided dense prediction with context-aware prompting. In *Proceedings of the IEEE/CVF conference on computer vision and pattern recognition*, pages 18082–18091, 2022. [2](#)
- [25] Mohammadreza Salehi, Niousha Sadjadi, Soroosh Baselizadeh, Mohammad H Rohban, and Hamid R Rabiee. Multiresolution knowledge distillation for anomaly detection. In *Proceedings of the IEEE/CVF conference on computer vision and pattern recognition*, pages 14902–14912, 2021. [5](#)
- [26] Domen Tabernik, Samo Šela, Jure Skvarč, and Danijel Skočaj. Segmentation-based deep-learning approach for surface-defect detection. *Journal of Intelligent Manufacturing*, 31(3):759–776, 2020. [5](#)
- [27] Nima Tajbakhsh, Suryakanth R Gurudu, and Jianming Liang. Automated polyp detection in colonoscopy videos using shape and context information. *IEEE transactions on medical imaging*, 35(2):630–644, 2015. [5](#)
- [28] Hugo Touvron, Thibaut Lavril, Gautier Izacard, Xavier Martinet, Marie-Anne Lachaux, Timothée Lacroix, Baptiste Rozière, Naman Goyal, Eric Hambro, Faisal Azhar, et al. Llama: Open and efficient foundation language models. *arXiv preprint arXiv:2302.13971*, 2023. [2](#)
- [29] Matthias Wieler and Tobias Hahn. Weakly supervised learning for industrial optical inspection. In *DAGM symposium in*, page 11, 2007. [5](#)
- [30] Hantao Yao, Rui Zhang, and Changsheng Xu. Visual-language prompt tuning with knowledge-guided context optimization. In *Proceedings of the IEEE/CVF conference on computer vision and pattern recognition*, pages 6757–6767, 2023. [2](#)
- [31] Hantao Yao, Rui Zhang, and Changsheng Xu. Tcpl: Textual-based class-aware prompt tuning for visual-language model. In *Proceedings of the IEEE/CVF Conference on Computer Vision and Pattern Recognition*, pages 23438–23448, 2024. [2](#)
- [32] Kaiyang Zhou, Jingkang Yang, Chen Change Loy, and Ziwei Liu. Conditional prompt learning for vision-language models. In *Proceedings of the IEEE/CVF conference on computer vision and pattern recognition*, pages 16816–16825, 2022. [2](#)
- [33] Qihang Zhou, Guansong Pang, Yu Tian, Shibo He, and Jiming Chen. Anomalyclip: Object-agnostic prompt learning for zero-shot anomaly detection. In *ICLR*, 2024. [1](#), [2](#), [4](#), [5](#)
- [34] Yang Zou, Jongheon Jeong, Latha Pemula, Dongqing Zhang, and Onkar Dabeer. Spot-the-difference self-supervised pre-training for anomaly detection and segmentation. In *European Conference on Computer Vision*, pages 392–408. Springer, 2022. [5](#)